# Telecom to mid-infrared spanning supercontinuum generation in hydrogenated amorphous silicon waveguides using a Thulium doped fiber laser pump source

**Utsav D. Dave,[1] Sarah Uvin,[1] Bart Kuyken,[1] Shankar Selvaraja,[2] Francois Leo,[1] Gunther Roelkens[1,*]**

[1]*Photonics Research Group – Center for nano- and biophotonics (NB-Photonics), Sint-Pietersnieuwstraat 41, B-9000 Ghent, Belgium*
[2]*imec, Kapeldreef 75, B-3001 Leuven, Belgium*
[*] *gunther.roelkens@intec.ugent.be*

**Abstract:** A 1000 nm wide supercontinuum, spanning from 1470 nm in the telecom band to 2470 nm in the mid-infrared is demonstrated in a 800 nm x 220 nm 1 cm long hydrogenated amorphous silicon strip waveguide. The pump source was a picosecond Thulium doped fiber laser centered at 1950 nm. The real part of the nonlinear parameter of this waveguide at 1950 nm is measured to be $100\pm10$ $W^{-1}m^{-1}$, while the imaginary part of the nonlinear parameter is measured to be $1.2\pm0.2$ $W^{-1}m^{-1}$. The supercontinuum is stable over a period of several hours, as the hydrogenated amorphous silicon waveguides do not degrade when exposed to the high power picosecond pulse train.

**OCIS codes:** (190.0190) Nonlinear Optics; (320.6629) Supercontinuum generation; (130.3130) Integrated optics materials.

## References and links

1. J. M. Dudley, G. Genty, and S. Coen, "Supercontinuum generation in photonic crystal fiber," Rev. Mod. Phys. 78, 1135-1184 (2006).
2. I. Hartl et al., "Ultrahigh-resolution optical coherence tomography using continuum generation in an air–silica microstructure optical fiber," Opt. Lett., vol. 26, no. 9, 608-610 (2001).
3. T. Morioka et al., "1 Tbit/s (100 Gbit/s×10 channel) OTDM/WDM transmission using a single supercontinuum WDM source," Electronics Letters, vol. 32, no. 10, 906-907 (1996).
4. T. Nakasyotani et al., "Wavelength-Division-Multiplexed Millimeter-Waveband Radio-on-Fiber System Using a Supercontinuum Light Source," Journal of Lightwave Technology, vol. 24, no. 1, 404-410 (2006).
5. C. F. Kaminski, "Supercontinuum radiation for applications in chemical sensing and microscopy," Applied Physics B 92, 367-378 (2008).
6. Y. Liu et al., "Broadband nonlinear vibrational spectroscopy by shaping a coherent fiber supercontinuum," Opt. Exp., vol. 21, no. 7, 8269-8275 (2013).
7. S. T. Sanders, "Wavelength-agile fiber laser using group-velocity dispersion of pulsed super-continua and application to broadband absorption spectroscopy," Appl. Phys. B 75, 799–802 (2002).
8. M. R. E. Lamont et al., "Supercontinuum generation in dispersion engineered highly nonlinear ($\gamma = 10$ /W/m) $As_2S_3$ chalcogenide planar waveguide," Opt. Exp., vol. 16, no. 19, 14938-44 (2008).
9. C. W. Rudy et al., "Octave-spanning supercontinuum generation in in situ tapered As2S3 fiber pumped by a thulium-doped fiber laser", Opt. Lett., vol. 38, no. 15, 2865-68 (2013).
10. R. Halir et al., "Ultrabroadband supercontinuum generation in a CMOS-compatible platform," Opt. Lett., vol. 37, no. 10, 1685-87 (2012).
11. C. R. Phillips et al., "Supercontinuum generation in quasi-phase-matched $LiNbO_3$ waveguide pumped by a Tm-doped fiber laser system," Opt. Lett., vol. 36, no. 19, 3912-14 (2011).
12. B. Kuyken et al., "Mid-infrared to telecom-band supercontinuum generation in highly nonlinear silicon-on-insulator wire waveguides," Opt. Exp., vol. 19, no. 21, 20172-20181 (2011).
13. B. Kuyken et al., "On-chip parametric amplification with 26:5 dB gain at telecommunication wavelengths using CMOS-compatible hydrogenated amorphous silicon waveguides", Opt. Lett., vol. 36, no. 4, 552-554 (2011).

14. B. Kuyken et al., "Nonlinear properties of and nonlinear processing in hydrogenated amorphous silicon waveguides," Opt. Exp., vol. 19, no. 26, B146-B153 (2011).
15. J. Matres et al., "High nonlinear figure-of-merit amorphous silicon waveguides," Opt. Exp., vol. 21, no. 4, 3932-40 (2013).
16. C. Grillet et al., "Amorphous silicon nanowires combining high nonlinearity, FOM and optical stability," Opt. Exp., vol. 20, no. 20, 22609-15 (2012).
17. G. P. Agrawal, Nonlinear Fiber Optics, Academic Press (2001).
18. G. Roelkens et al., "Silicon-based heterogeneous photonic integrated circuits for the mid-infrared," Opt. Mat. Exp., vol. 3, no. 9, 1523-36 (2013).
19. H. K. Tsang et al., "Two-photon absorption and self-phase modulation in InGaAsP/InP multi-quantumwell wave-guides," J. Appl. Phys. 70(7), 3992–3994 (1991).
20. L. Shen et al., "Nonlinear transmission properties of hydrogenated amorphous silicon core fibers towards the mid-infrared regime," Opt. Exp., vol. 21, no. 11, 13075-83 (2013).
21. Yin et al., "Impact of two-photon absorption on self-phase modulation in silicon waveguides", Opt. Lett., vol. 32, no. 14, 2031-33 (2007).
22. F. Leo et al., "Measurement and tuning of the chromatic dispersion around the half band gap spectral region of a silicon photonic wire", submitted to Optics Letters.

## 1. Introduction

The mid-infrared (mid-IR) wavelength range, which is generally considered to span wavelengths in the 2-20 μm range, is of key interest for various sensing and spectroscopy applications, since many molecules have characteristic absorption bands in this wavelength range. One of the great challenges in developing mid–IR systems for various applications is the lack of practical sources and detectors. Nonlinear optics provides a good way to generate new optical frequencies spaced a predictable and controllable distance from a strong pump frequency and is thus well-placed to take advantage of commercially available sources at shorter wavelengths to generate mid-IR spatial and/or temporally coherent radiation. Supercontinuum generation (SCG) has received a lot of attention from researchers in recent years [1] because of the breadth of its potential applications such as in optical coherence tomography [2], wavelength division multiplexing in telecommunications [3,4], in optical sensing [5] and in spectroscopy [6,7]. A lot of the work in supercontinuum generation has focused on the use of photonics crystal fibers [2]. The ability to tailor the dispersion profile of such fibers with high precision enables the generation of large bandwidth supercontinuum spectra. On-chip supercontinuum generation – which could make it lower cost, more robust and more power efficient compared to the microstructured fiber approach – has been achieved on various waveguide platforms including chalcogenide [8,9], silicon nitride [10], lithium niobate [11] and silicon [12]. Implementing nonlinear optical functionality in silicon photonic integrated circuits has many advantages since it provides tight confinement due to the high index contrast, resulting in high waveguide intensities for modest optical power levels. The high index contrast allows for dispersion engineering of the waveguides, a critical feature for efficient nonlinear interaction. Waveguides can be fabricated with relatively low loss (~ 0.5-2 dB/cm) using CMOS-compatible processes, resulting in a potential interaction length of several centimeters, which combined with the very high nonlinear parameter enables strong nonlinear interaction. However, two-photon absorption (TPA) can be a problem when working with high optical intensities since not only does TPA directly cause losses, but also the resulting free carriers lead to more nonlinear losses through free carrier absorption. Therefore, for crystalline silicon where the half bandgap wavelength lies at 2.2 μm, one has to work close to or beyond this wavelength to avoid these nonlinear losses. This requires the use of bulky optical parametric oscillator systems as a pump source, which hampers the development of compact and low-cost systems. Hydrogenated amorphous silicon waveguides on the other hand, are known to have a similar index contrast and nonlinear index as crystalline silicon [13] but the material has a higher bandgap, enabling the pump to be located at shorter wavelengths where, for example, compact Thulium-based fiber sources are now

commercially available. This way one can work with higher powers than is usually possible at telecom wavelengths without suffering from the adverse effects of TPA. In [14] we reported that the amorphous silicon material can be unstable if pumped in the 1550 nm wavelength range due to what is known as the Staebler-Wronski effect, which causes degradation of the material through breaking of the Si-Si bonds. This effect is also minimized by working at a pump wavelength of 1950 nm because the bonds purportedly break due to electron-hole pairs recombining after having been created via TPA. However, this effect seems to be related to the material deposition technique, as other groups have reported stable operation at 1550 nm [15, 16]. Supercontinuum generation in the 1.5-2.5 μm wavelength range is of high importance for the spectroscopic analysis of water-rich fluids, given the relatively low absorption of water in this wavelength range and the existence of overtone transitions of many molecular bonds in this wavelength range. From the above discussion, the use of hydrogenated amorphous silicon waveguides in combination with a Thulium-based fiber sources as the pump is a promising approach for this application. In this paper we elaborate on the generation of a 1.47 μm to 2.47 μm spanning supercontinuum using a picosecond pulsed Thulium-based fiber source in hydrogenated amorphous silicon waveguides. The device performance is compared to similar devices implemented on a crystalline silicon photonics platform.

## 2. Supercontinuum generation

Supercontinuum generation with a picosecond pulsed pump source is mostly mediated by four-wave mixing (FWM) and the associated rise of modulation instability bands from noise [1]. The position of these modulation instability (MI) side lobes is determined by the dispersion characteristics of the waveguide. In general, anomalous group velocity dispersion (GVD) is required for the phase matching of the MI bands which are close to the pump frequency. However, one can also generate MI bands farther away from the pump wavelength when taking into account the higher order dispersion terms. These bands grow from noise and consequently, the position of the band peak is wherever the gain is at its maximum, i.e. where perfect phase matching is obtained. The degenerate four-wave mixing mechanism in the undepleted pump approximation describes the initial experimental situation. The phase mismatch between the linear propagation constants of the pump and the generated idler and signal frequencies is compensated for by the nonlinear phase mismatch arising from self- and cross-phase modulation (SPM and XPM) as given by Eq. 1 below [17].

$$\Delta k + 2.\mathrm{Re}(\gamma)P = k_s + k_i - 2k_p + 2.\mathrm{Re}(\gamma)P = \beta_2 \Delta\omega^2 + \frac{1}{12}\beta_4 \Delta\omega^4 + 2.\mathrm{Re}(\gamma)P \qquad (1)$$

Here, $k_p$, $k_s$ and $k_i$ are the linear propagation constants at the pump, signal and idler frequencies respectively. $\Delta\omega$ is the frequency offset of the idler (or signal) from the pump and $\beta_2$ and $\beta_4$ are the GVD and 4th order dispersion term respectively. $2Re(\gamma)P$ is the nonlinear phase mismatch due to SPM and XPM and $P$ is the peak power of the pump. $Re(\gamma)$ is the real part of the nonlinear parameter $\gamma$ as defined by Eq. 2 below where $k_0$ is the propagation constant in vacuum, $n_2$ the Kerr nonlinear index of the material, $A_{eff}$ is the effective area of the waveguide and $\beta_{TPA}$ is the two-photon absorption coefficient.

$$\gamma = \frac{k_0 n_2}{A_{eff}} + i \frac{\beta_{TPA}}{2 A_{eff}} \qquad (2)$$

As one can see from Eq. 1, the $\beta_4$ term can be ignored for small frequency separations and we get the condition that the GVD has to be anomalous ($\beta_2 < 0$) for materials with a positive

nonlinear parameter $Re(\gamma)$, resulting in a phase matched wavelength band close to the pump (labeled MI1 in this paper). At higher values of $\Delta\omega$, the $\beta_4$ term has to be taken into consideration. This way, along with the condition of anomalous GVD, another phase matched wavelength band far away from the pump occurs if $\beta_4 > 0$ [18]. This second modulation instability band (labeled MI2 in this paper) is what allows for the wide breadth of the generated supercontinuum. Of course, there is self-phase modulation mediated broadening, but at picosecond pump durations, this broadening is much smaller compared to the overall experimentally observed breadth of the supercontinuum.

For the experiment, a Thulium doped modelocked fiber laser from AdValue Photonics with a pulse duration of 1.24ps (full width at half maximum) and a pulse repetition rate of 26 MHz is used. Highly nonlinear hydrogenated amorphous silicon (a-Si:H) photonic wires were defined by depositing a 220 nm a-Si:H layer on top of a 1950 nm polished silicon dioxide layer on a silicon substrate in a CMOS pilot line. The photonic wires were patterned using wafer-scale CMOS fabrication technology. The inset of Fig. 1 shows the scanning electron microscope (SEM) cross section of the waveguide used in the experiment which has average width of 792 nm and a height of 218 nm as measured by the SEM. The pump laser is coupled to the fundamental quasi-TE mode of the waveguide using a surface etched grating coupler (grating period 1040 nm, duty cycle 50%, -12 dB coupling efficiency at 1950 nm for TE polarization under a 25 degree fiber angle), while the waveguide output is collected using a lensed fiber and connected to a mid-IR optical spectrum analyzer. The source is passed through a polarizer and polarization rotator in order to ensure maximum coupling to the waveguide fundamental TE mode. As shown in Fig. 1, at a coupled peak power in the waveguide of 7.6 W, the MI1 side lobes appear on the output spectra. With an increase in power the second pair of MI2 side lobes appears farther away from the pump. As power is increased further, these bands merge and create a continuum. With increasing power, the supercontinuum broadens until it is 1000 nm wide as shown in the final plot of Fig. 1. The MI2 side lobe on the long wavelength side is less visible because of the higher losses experienced by the longer wavelengths in the standard single mode fibers used for coupling out of the waveguide to the spectrum analyzer.
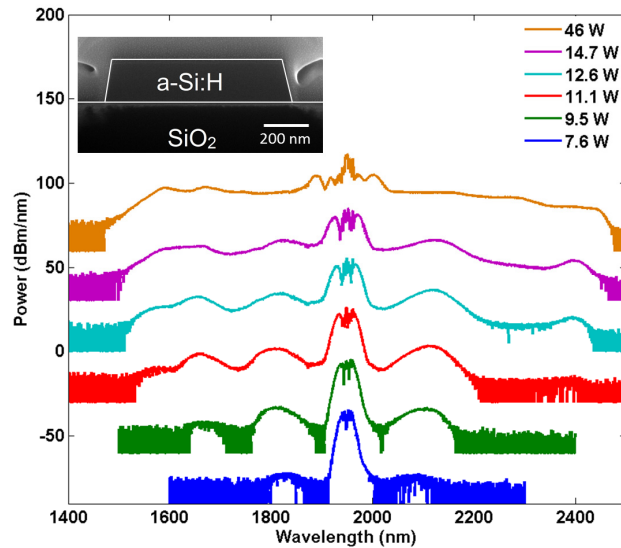


Figure 1 – The build-up of the supercontinuum with increasing power. MI1 bands appear at 7.6 W peak power, MI2 at 9.5 W and at 11.1 W the bands merge to form the supercontinuum which then grows as power is increased to 12.6 W and 14.7 W and it finally saturates when the spectral width is about 1000 nm at 46 W. Successive plots are shifted by 20dB for clarity. The inset shows the SEM cross-section of the waveguide used in the experiment.

## 3. Characterization of the a-Si waveguide parameters

In order to quantitatively compare the amorphous silicon platform to earlier reported results, the waveguide nonlinear parameter and material stability were investigated. Below, we describe the results of those characterizations.

### 3.1 Material stability

It has been reported previously in [14] that the amorphous silicon material is not stable against exposure to high optical intensity at 1550 nm, which leads to material degradation. This effect was attributed to the breaking of weak Si-Si bonds in the material mediated by the recombination of carriers created by two-photon absorption. Thus, working at longer wavelengths should significantly decrease the TPA and consequently, the material degradation. Indeed this is what was observed, as shown in Fig. 2 where the supercontinuum is maintained for several hours without any significant degradation of the spectrum, even though the peak power coupled into the waveguide was 60±10W. This makes the use of hydrogenated amorphous silicon waveguides appealing for real-life applications.
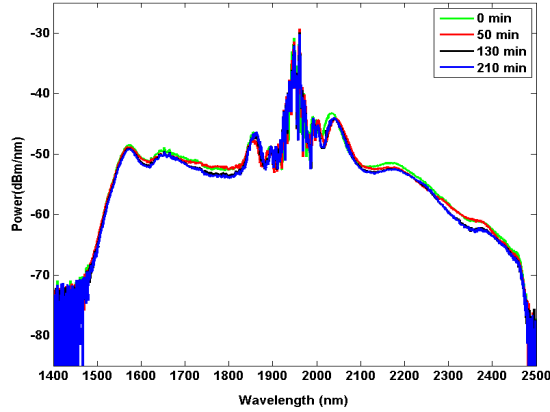


Figure 2 – Stability of the generated supercontinuum with time demonstrating that the hydrogenated amorphous silicon material is stable at the 1950nm pump wavelength. The peak power in the waveguide is 60±10 W.

### 3.2 TPA measurement for Im(γ) determination

In order to measure the two-photon absorption in the hydrogenated amorphous silicon waveguides at 1950 nm wavelength, the reciprocal of the optical transmission through such a waveguide was measured as a function of peak input power. From [19], we can relate the TPA coefficient to the inverse of the transmission using Eq. 3:

$$\frac{1}{T} = \frac{P_{IN}}{P_{OUT}} = \exp(\alpha_{LIN}L)\frac{L_{eff}}{A_{eff}}\beta_{TPA}P_{IN} + \exp(\alpha_{LIN}L)$$

(3)

Here, $\alpha_{LIN}$ is the linear loss coefficient which is measured to be 0.51 cm$^{-1}$ by the cut-back method, $L$ is the waveguide length and $L_{eff}$ is the effective length defined as $(1 - \exp(-\alpha_{LIN}L))/\alpha_{LIN}$ to take into account the linear propagation loss. Fig. 3 below shows the results of the transmission measurement with increasing input peak powers. From the slope of the linear fit in Fig. 3(b), $Im(\gamma)$ is calculated to be 1.2±0.2 W$^{-1}$m$^{-1}$, which from Eq. 2 gives $\beta_{TPA}$ = 2.3x10$^{-13}$ mW$^{-1}$. This matches well with the value reported in [20] for the same wavelength. Compared with the value of the $Im(\gamma)$ reported in [14] at 1550 nm wavelength (28

W$^{-1}$m$^{-1}$), the value obtained in the current experiment is significantly lower which accounts for the material stability observed in Fig. 2.



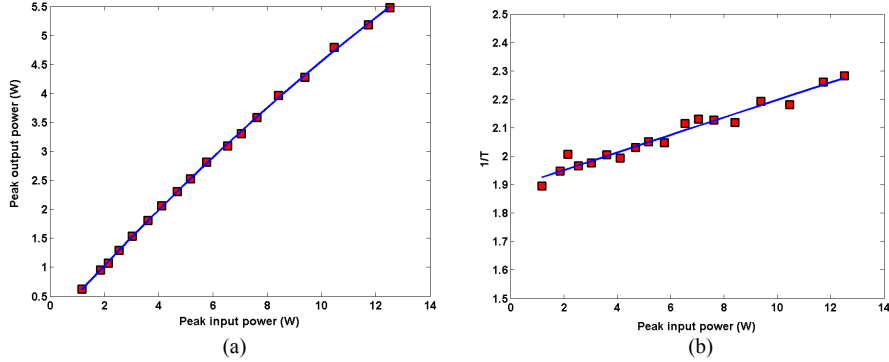(a)                                                                 (b)

Figure 3 – (a) Plot of the peak powers coupled out of the waveguide versus input peak power, which shows a not perfectly linear relation. (b) Plot of the inverse transmission and a linear fit, which gives a value for the two-photon absorption coefficient of the amorphous silicon material of $\beta_{TPA} = 2.3\text{x}10^{-13}$ mW$^{-1}$.

## 3.3 Determination of Re(γ)

A measurement of the self-phase modulation of the pump was made to measure the value of the real part of the nonlinear parameter γ. Fig. 4 shows the SPM measurements and the comparison to simulation of the nonlinear Schrödinger equation by the split-step Fourier transform method which included carrier effects [21]. This gives a value for Re(γ) of 100±10 W$^{-1}$m$^{-1}$.
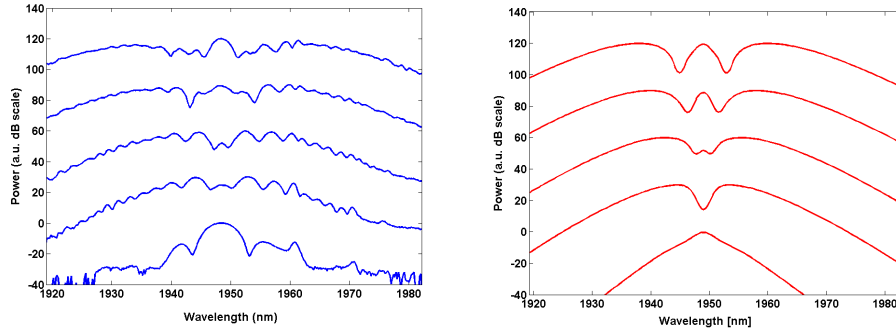


Figure 4 – Measured spectra (left) for the determination of Re(γ) with coupled peak powers of 1.9 W, 6.1 W, 7.6 W, 9.5 W and 11.1 W and the simulations of the nonlinear Schrödinger equation (right) gives Re(γ) = 100 W$^{-1}$m$^{-1}$. Successive plots are shifted by 30dB for clarity.

Taking this value of Re(γ) and considering the positions of the MI1 and MI2 bands in Fig. 1, we can infer the values of $\beta_2$ and the $\beta_4$ using eq. 1. Thus, at the pump wavelength of 1950 nm, we get $\beta_2$ = -0.4 ps$^2$/m and get $\beta_4$ = 1.3x10$^{-4}$ ps$^4$/m. Simulations of the dispersion of the waveguide using the finite difference method were carried out in this wavelength range to confirm this $\beta_2$ value. It is known from previous work [22] that simulations are not accurate enough to provide $\beta_4$ values. Since the material dispersion of amorphous silicon is unknown, we assumed the material dispersion of crystalline silicon. From these simulations, a waveguide of dimensions 832 nm x 212 nm is found to match the experimental value of $\beta_2$. The dimensions of the simulated waveguide lie within 5% error of the measured dimensions in Fig. 1 and the difference is thought to be due to the material dispersion of amorphous silicon being different from that of the crystalline silicon.

## 4. Supercontinuum generation in crystalline silicon waveguides

In order to demonstrate the large performance benefits from amorphous silicon waveguides for this application, supercontinuum generation in a crystalline silicon waveguide with nominally identical waveguide dimensions was also investigated. As shown in Fig. 5, the positions of the MI1 and MI2 side lobes show that the dispersion in the crystalline waveguide is similar to that of the amorphous waveguide. Clearly, amorphous silicon provides a much broader supercontinuum at similar power levels, even when the waveguide dimensions, linear loss and dispersion are all comparable to the hydrogenated amorphous silicon waveguide. This is because of the higher TPA coefficient of the crystalline silicon at this wavelength (about 4 times higher), which makes it unable to support a similarly wide supercontinuum.
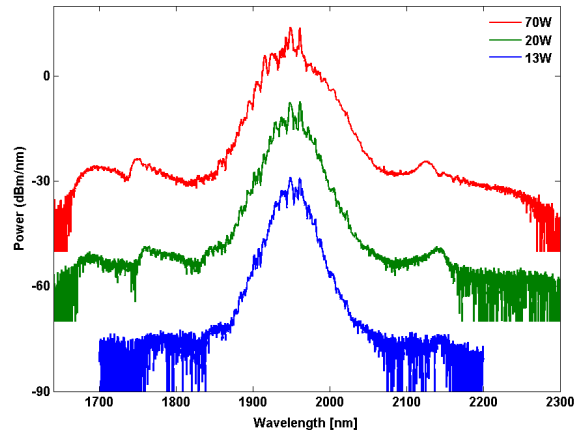


Figure 5 – Supercontinuum generation in crystalline silicon waveguides. The positions of the modulation instability bands of a crystalline silicon waveguide with the same dimensions as the one used for the supercontinuum generation in a-Si:H show that the dispersion of this waveguide is similar. Clearly, a-Si:H is a better material system for supercontinuum generation at this wavelength. Successive plots are shifted by 20dB to make them clearer.

## 5. Conclusions

We have reported broadband supercontinuum generation in an amorphous silicon waveguide spanning from 1470 nm to 2470 nm. By pumping the waveguide at 1950 nm wavelength using a commercially available picosecond laser source, we take advantage of the very low TPA coefficient in hydrogenated amorphous silicon. Contrasting this with the broadening observed in a crystalline silicon waveguide of the same dimensions, similar loss and dispersion, clearly the amorphous silicon provides a much broader supercontinuum at similar power levels. The amorphous material is also shown to be stable when exposed for several hours continuously to the high peak powers required for the supercontinuum generation. Hydrogenated amorphous silicon is thus brought forth as a promising material for on-chip nonlinear optics.

## Acknowledgements